HHS Public Access

Author manuscript

Rev Sci Instrum. Author manuscript; available in PMC 2015 November 13.

Published in final edited form as:

Rev Sci Instrum. 2012 August ; 83(8): 085103. doi:10.1063/1.4739768.

Cavity ring-down spectroscopy with an automated control feedback system for investigating nitrate radical surface chemistry reactions

Michael M. Flemmer and **Jason E. Ham**[a]

Exposure Assessment Branch, Health Effects Laboratory Division, National Institute for Occupational Safety and Health, 1095 Willowdale Road, Morgantown, West Virginia 26505, USA

Abstract

Nitrate radical ($NO_3^•$) surface chemistry of indoor environments has not been well studied due to the difficulty in generating and maintaining $NO_3^•$ at low concentrations for long term exposures. This article presents the Surface Chemistry Reactant Air Delivery and Experiment System (SCRADES), a novel feedback controlled system developed to deliver nitrate radicals at specified concentrations (50–500 ppt, ±30 ppt) and flow rates (500–2000 ml min^{-1}) to a variety of indoor surfaces to initiate reaction chemistry for periods of up to 72 h. The system uses a cavity ring-down spectrometer (CRDS), with a detection limit of 1.7 ppt, to measure the concentration of $NO_3^•$ supplied to a 24 l experiment chamber. Nitrate radicals are introduced via thermal decomposition of N_2O_5 and diluted with clean dry air until the desired concentration is achieved. Additionally, this article addresses details concerning $NO_3^•$ loss through the system, consistency of the $NO_3^•$ concentration delivered, and stability of the CRDS cavity over long exposure durations (72 h).

I. Introduction

A recent review by Weschler highlighted research progress in the last 20 years to characterize the dynamic nature of the indoor environment.[1] This review focused on indoor chemistry and revealed that there are still several fundamental questions regarding indoor gas-phase and surface-phase chemistry. The article discusses the multitude of experimental evidence demonstrating that several initiator species such as ozone (O_3), hydroxyl radicals ($OH^•$), and nitrate radicals ($NO_3^•$) are present indoors and can react with volatile/semi-volatile organic compounds (VOCs/SVOCs) to produce oxygenated organic compounds such as: aldehydes, ketones, carboxylic acids, dicarbonyls, and organic nitrates.[2–9] Although the gas-phase chemistry of these indoor initiators with VOCs/SVOCs has been studied extensively, the equivalent reactions on a variety of surfaces are still poorly understood. Furthermore, nitrate radical reactions are the least studied of these reactants due to the difficulties in generating $NO_3^•$ for flow studies, measuring $NO_3^•$ concentrations, and delivering known concentrations of $NO_3^•$ for long term experiments.

[a]Author to whom correspondence should be addressed. bvo2@cdc.gov. Tel.: 1-304-285-6214. Fax: 1-304-285-6041.

The nitrate radical ($NO_3^{\bullet}$) has been identified as the main reactive species in the nighttime outdoor environment[10, 11] and has been recently measured in the indoor environment.[12] A variety of sensitive analytical techniques have previously been employed to measure $NO_3^{\bullet}$ such as laser-induced fluorescence,[13–17] direct optical absorption spectroscopy,[18–24] Fourier-transform infrared spectroscopy,[25] and cavity ring-down spectroscopy (CRDS).[26–31] These measurements have been made due to an interest in measuring the transient nighttime concentrations of $NO_3^{\bullet}$ in the atmosphere, which can be in the sub-parts-per-trillion (ppt) to hundreds of ppt range. Over the last two decades, CRDS has gained popularity due to its high sensitivity and ability to monitor localized $NO_3^{\bullet}$ concentration fluctuations compared to long-path spectroscopy techniques. Recently, $NO_3^{\bullet}$ measurements were made indoors using a surrogate mass spectrometric technique based on the reaction of cyclohexene + $NO_3^{\bullet}$ and measuring the yield of cyclohexane nitrate.[12] Using this technique, Nøjgaard was able to measure $NO_3^{\bullet}$ concentrations indoors from 1 to 58 ppt.

There have been only a few studies of the reactions of VOCs/SVOCs + indoor reactant ($OH^{\bullet}$, O_3, or $NO_3^{\bullet}$) on surfaces found in indoor environments.[32–42] These studies have focused on surface reactions of VOCs derived from material emissions and reactions of indoor surfaces that have been coated with consumer cleaning products. Recently, our group developed a novel computer controlled feedback system, Field and Laboratory Emission Cell (FLEC) Automation and Control System (FACS) that could be used to deliver air mixed with a specified concentration of O_3 at flow rates up to 2 l min^{-1} and at a relative humidity between 5% and 90%.[43] This system has been used to investigate the surface reactions of O_3 with two terpene alcohols (*α*-terpineol, dihydromyrcenol) and one consumer based pine-oil cleaner on glass and vinyl flooring tiles.[35–37] Using this system, several new oxygenated products were observed compared to gas-phase product experiments indicating that surfaces can stabilize reaction intermediates and/or catalyze reactions to generate new oxidation products.

In this article, the development of a new feedback system, which delivers nitrate radicals ($NO_3^{\bullet}$) to a surface at specified concentrations, relative humidity, and flow rate, will be discussed. The new system, although based on the previous FACS, incorporates: (1) $N_2O_5/NO_3^{\bullet}$ introduction, (2) cavity ring-down spectroscopy to measure $NO_3^{\bullet}$ concentrations, (3) new feedback controls, and (4) a newly developed Teflon experiment chamber for surface chemistry experiments. This article will discuss steps to generate $NO_3^{\bullet}$, calibration and stability measurement results, and how this system will be used to initiate $NO_3^{\bullet}$ + VOC/SVOC reactions on a variety of indoor surfaces.

II. Instrument

A. Overview

The new Surface Chemistry Reactant Air Delivery and Experiment System (SCRADES) (Figure 1) is based on the previous FACS[43] and is composed of three stages: the air purification stage, the air humidification stage, and the reactant injection and delivery stage. The air purification and air humidification stages have been previously described[35–37,43] and remain unchanged from the original system except for modifications allowing for higher flow rates. The redesigned reactant injection and delivery stage begins by introducing $NO_3^{\bullet}$

into the air stream. After two dilution steps, the CRDS measures the $NO_3^{\bullet}$ concentration, after which the air continues to the experiment chamber.

The entire system is controlled by a standard desktop computer which houses an analog output card, a multifunction data acquisition card, a multi-port serial card, and a highspeed analog data acquisition card. An additional analog output device and a digital input/output device are connected to the computer via Universal Serial Bus (USB) ports. The control program is a modified version of the original C/C++ Windows application that was written in-house and utilizes libraries provided by both National Instruments Corp. (NI) (Austin, TX) and Gage-Applied (Lockport, IL).

B. Design and assembly

1. N_2O_5 synthesis and transfer—Nitrate radicals are generated by thermal decomposition of N_2O_5 using a similar method as described by Atkinson *et al.*[3] N_2O_5 (white, crystalline solid) is synthesized via mixing 0.5% NO_2 (from a commercial gas cylinder) at 1.01 min^{-1} with O_3 at 1.01 min^{-1} generated at 1.25 g h^{-1} (OSR-4, Ozone Solutions, Sioux Center, IA) using zero grade air into a 1.2 l mixing tube (Ace glass, Vineland, NJ) as seen in reactions 1 and 2. The NO_2/O_3 mixture was allowed to flow from the mixing tube into a glass vacuum trap (8750-20, Ace glass, Vineland, NJ) which was partially submerged in an ethanol bath held at −75 °C. N_2O_5 was stored in the −75 °C bath until use in the feedback system. To minimize its surface loss by conversion to nitric acid, N_2O_5 was used within six days after synthesis.[44]

$$O_3 + NO_2 \rightarrow N_2O_5 \quad \text{(Reaction 1)}$$

$$N_2O_5 \leftrightarrow NO_3^{\bullet} + NO_2 \quad \text{(Reaction 2)}$$

For CRDS experiments, the N_2O_5 trap was moved to another ethanol bath held at −40°C (±0.5 °C). This was done to increase the vapor pressure of N_2O_5 above the solid to 0.55 Torr.[45] Ultrahigh purity (UHP) N_2, beginning at 10.0 ml min^{-1}, is then used to sweep $N_2O_5/NO_3^{\bullet}$ into the CRDS cavity. However, at this pressure, the concentration of N_2O_5 that is generated is ∼945 ppm (63 ppm $NO_3^{\bullet}$), which is considerably greater than indoor measurements made by Nøjgaard (<60 ppt).[12] As a consequence, serial dilution was incorporated using two mixing cavities. $N_2O_5/NO_3^{\bullet}$ from the trap is mixed with clean, dry air at a ratio of 1:100 into a 1.18 l borosilicate glass column (Mix Air 1). The reduced $N_2O_5/NO_3^{\bullet}$ concentration was further diluted using clean, dry air at a ratio 1:49 in a 79 ml borosilicate glass column (Mix Air 2) before delivery to the CRDS optical cavity. All mixing cavities and the optical cavity are at room temperature, typically 295–298 K. At these temperatures, the ratio of $N_2O_5/NO_3^{\bullet}$ is ∼15:1.[16]

Based on the $NO_3^{\bullet}$ concentration derived from the CRDS, the airflows are adjusted to meet the target concentration (100 ppt, ±30 ppt). Large, coarse concentration adjustments are made by altering the flows through the second stage dilution chamber (Mix Air 2) while fine adjustments are made by altering the flow of UHP N_2 through the trap. Additionally, in order to reduce the loss of $NO_3^{\bullet}$ due to photolytic degradation, the dilution system and the

CRDS are in a light tight enclosure. All of the tubing outside of the enclosure has been incased in black heat-shrink tubing.

Initially, an attempt was made to generate $NO_3^{\bullet}$ in a constant flow system by introducing NO_2 (150 ppb) and O_3 (75 ppb) into a 1 1 mixing tube at 300 ml min^{-1}. However, given the formation rate of $NO_3^{\bullet}$ at 7.87×10^{-7} ppb^{-1} s^{-1} and the residence time of the mixing cavity, only 2.1% of the O_3 reacted. Given these parameters, the amount of $NO_3^{\bullet}$ that can be generated at room temperature is ~13 ppt. Although this $NO_3^{\bullet}$ concentration lies in the regime of both the predicted and measured range, the ability to generate $NO_3^{\bullet}$ consistently without fluctuations in concentration was difficult. Also, due to an absorption band in the 662 nm region, large concentrations of NO_2 could interfere with measurements of $NO_3^{\bullet}$ as described below. For this reason, solid N_2O_5 was synthesized and transferred to the optical cavity as described above.

2. CRDS

a. CRDS theory: CRDS has been reviewed extensively,[28,46–52] so only a brief description will be given here. This absorption technique is based on measuring the loss of light over time in an optical cavity constructed of two highly reflective mirrors (typically, $R > 99.990$) and is given by the equation $I(t) = I_o \exp^{(-t/\tau)}$, where I_o = initial intensity of light, t = time, and τ is the ring-down time.

A CRDS measurement consists of a short duration of light (100 μs for this system) injected into an optical cavity and then observing the intensity decay over time. This measurement of the characteristic decay time constants in the presence and absence of an absorber (i.e., $NO_3^{\bullet}$) yields its concentration for a known absorption cross section (σ), and is calculated using a derivation of Beer's Law, Eq. (1), where α is the absorption coefficient (cm^{-1}), σ is the absorption cross section (cm^2 $molecule^{-1}$), R_L is the ratio of the cavity length (L) to the length over which the absorber is present (L_A), c is the speed of light, and τ_{NO3} and τ_{empty} are the ring-down times with and without the presence of absorber

$$\alpha = [NO_3]\sigma = \frac{R_L}{c}\left(\frac{1}{\tau_{NO_3}} - \frac{1}{\tau_{empty}}\right). \quad (1)$$

b. CRDS system design: The CRDS system consists of a diode laser, optical isolator, Teflon optical cavity, two highly reflective mirrors, and a photomultiplier tube (PMT). A 662± 0.4 nm continuous wave diode laser (IQμ1H, Power Technology, Inc., Little Rock, AR), modulated at a frequency of 1500 Hz with a 15% duty cycle, passes through an optical isolator (IO-3-662-LP, OFR/Thorlabs, Verona, NJ) and into a 1.0 in. i.d. × 24.0 in. Teflon tube which forms the optical cavity. The ends of the optical cavity consist of two 1.0 in. highly reflective mirrors (R > 99.995, radius of curvature = 1 m, Advance Thin Films, Boulder, CO) which are held by custom designed Delrin mounts connected to the cavity via steel bellows (150-96-3-l, Standard Bellows Co., Windsor Locks, CT). The mirror alignment is adjusted using Starrett (Athol, MA) 263L micrometer heads. A set of tension springs maintains the integrity and stability of the mirror mounts and the alignment heads. The light

exiting the optical cavity is detected using an 8 MHz PMT (H10492-013, Hamamatsu Corp., Bridgewater, NJ). The PMT signal is captured by a Gage-Applied 14-bit data acquisition card (Octopus CompuScope 8327, Lockport, IL) which is triggered by the laser modulation signal. There are two main sources of signal noise. The first derives from the 8 MHz bandwidth of the PMT. The second comes from the building electrical system and appears as low amplitude 60 Hz ripple. Therefore, the 1500 data records from a one second event are averaged in order to reduce this signal noise, then processed to determine the ring-down time. When the optical cavity was evacuated to 50 Torr, the empty cavity ring-down time was measured to be 173 μs.

There are several interferences that are inherent with measuring $NO_3^{\bullet}$ concentrations by CRDS at 662 nm. The absorption cross section ($\sigma_{NO_3^{\bullet}}$ at 662 nm) is 2.1×10^{-17} cm^2 molecule^{-1} at 298 K; however, there is also a small absorption by NO_2 (a byproduct of N_2O_5 decomposition), $\sigma_{NO_2} = 5.6 \times 10^{-21}$ cm^2 molecule^{-1} at 298 K.[53] The four orders of magnitude difference in absorption cross sections reduce the impact of NO_2 on the measured ring-down time. As seen in reaction (2), thermal decomposition of N_2O_5 generates $NO_3^{\bullet}$ and NO_2 in a 1:1 ratio. Given this, the concentration of NO_2 contributes approximately 0.1%–0.2% to the measured ring-down time. Residual N_2O_5 from incomplete decomposition has a negligible absorption cross section of $\sigma_{N_2O_5} = 1.0 \times 10^{-24}$ cm^2 molecule^{-1} at 298 K.[53] Water may also interfere with the ring-down time due to absorption lines ($\sigma_{N_2O} = 1.06 \times 10^{-26}$ cm^2 molecule^{-1}) at 662 nm. Since τ_{empty} is determined using the same relative humidity as the experiment, this interference becomes incorporated into the background for subsequent concentration measurements. Furthermore, hydrolysis reactions of N_2O_5 may be catalyzed on surfaces at higher humidity. Therefore, all experiments thus far have been done at 5% RH.[10]

3. Teflon experiment chamber—Due to the reactivity of $NO_3^{\bullet}$ with water absorbed to stainless steel and the possible production of nitric acid, a new inert experiment chamber was designed. The chamber consists of a black anodized aluminum box, measuring 15 in. × 15 in. × 6.5 in. (38.1 cm × 38.1 cm × 16.5 cm) inside, with all of the interior surfaces lined with 2-mil Teflon sheeting (American Durafilm, Hollistan, MA). The internal volume of the chamber is ∼23.97 1 and has an air-exchange rate of 1.25 h^{-1} at 500 ml min^{-1}. The $N_2O_5/NO_3^{\bullet}$ air mixture enters the top of the chamber at the center via a Teflon nozzle designed to evenly distribute the air/$NO_3^{\bullet}$ mixture to the surface. The test surface rests on a Teflon support plate with raised sides, in order to minimize edge exposure to the reactant. The test bed sits in the center of the chamber and rests on a Teflon pedestal that doubles as the exhaust port. The gas mixture exits the bottom of chamber from the center and proceeds to the collection system, as previously described.[35–37,43]

C. Control

As stated above, the system is controlled by a desktop computer with four additional Peripheral Component Interconnect (PCI)-bus cards installed. The additional cards consist of one NI PCI-6040E Multifunction I/O Data Acquisition board, one NI PCI-6713 Analog Output board (National Instruments Corp., Austin, TX), one Sealevel Systems (Liberty, SC) Comm+8.LPCI eight-port serial board, and the aforementioned Gage-Applied card.

The computer runs an application that was written using Microsoft (Redmond, WA) Visual C/C++ 6.0. This application allows the researcher to define the parameters of the experiment such as flow rate through the experiment chamber, relative humidity of the experiment air, target $NO_3^{\bullet}$ concentration, duration of the experiment, and the recording interval for data collection. The system continually monitors all parameters and makes adjustments accordingly. A proportional-integral-differential (PID) algorithm controls the adjustment of the $NO_3^{\bullet}$ concentration. Due to the low flow rates, mixing chamber sizes, and CRDS cavity size, there is a lag time of nearly 3 min between adjustments and the detection of concentration changes. The air temperature and humidity are measured using the in-house developed in-line sensor units described previously.[43]

III. Experiments

A. $NO_3^{\bullet}$ loss through system

Previous reports have shown that $NO_3^{\bullet}$ can react with water absorbed to metal surfaces and/or be removed by decomposition/reaction on Teflon walls.[29,30,54] Dube *et al.* observed a first order loss rate of $NO_3^{\bullet}$ on the Teflon inlet walls of their CRDS instrument of approximately 0.2 s^{-1}.[29] To determine the potential loss of $NO_3^{\bullet}$ throughout the system described here, three-way Teflon solenoid valves were temporarily installed to allow alternate air flow paths. First, air flowed through the system as originally described with the amount of N_2 going through the N_2O_5 trap set to a constant flow rate. Once the system achieved stability, the concentration and ring-down time were recorded. The flow was then altered so that air flowed from the mixing chambers, through the experiment chamber, and then to the CRDS. When the new flow path regained stability, the new concentration and ring-down times were recorded.

This series of experiments were performed using UHP N_2 flow rates of 5, 10, and 15 ml min^{-1} through the N_2O_5 trap while flows through both dilution chambers were held constant. Using this data, a loss curve was generated allowing the determination for the required concentration of $NO_3^{\bullet}$ through the CRDS cavity in order to have the specified concentration of reactant delivered to a surface inside the experiment chamber. The percent loss of $NO_3^{\bullet}$ at each flow rate was determined five times for statistical analysis. This relationship was used to calculate the required concentration of $NO_3^{\bullet}$ within the CRDS in order to achieve the target concentration inside the chamber.

B. Stability profiles of CRDS: τ_{empty} and $\tau_{NO_3^{\bullet}}$

The $NO_3^{\bullet}$ concentration is calculated every 5 s using a stored τ_{empty} value that is measured before an experiment has begun. However, if τ_{empty} drifts as a function of time, then the calculated $NO_3^{\bullet}$ concentrations will have an associated error due to this drift. In typical CRDS measurements of $NO_3^{\bullet}$, NO is added as a titrant to remove $NO_3^{\bullet}$ from the cavity so that τ_{empty} can be periodically determined throughout a measurement. This reaction occurs quickly with a rate constant of 2.6×10^{-11} cm^3 $molecule^{-1}$ s^{-1} and results in the formation of $2NO_2$ molecules. Unfortunately, this additional NO_2 to the system may interfere with surface chemistry experiments as well as introduce an error to the CRDS ring-down time. Furthermore, the system is designed to provide continuous specified concentrations of $NO_3^{\bullet}$

for up to 72 h without interruptions in flow which would occur with periodic injections of NO. To determine the amount of drift in the system, a series of τ_{empty} measurements were collected and analyzed to determine its stability profile. τ_{empty} was determined five times at a flow rate of 500 ml min^{-1} and 5% relative humidity over 72 h.

IV. Results and Discussion

A. Detection of $NO_3^•$

Using the CRDS system described above, ring-down times were collected with $NO_3^•$ (τ_{NO_3}) and without $NO_3^•$ (τ_{empty}) present. The natural logs of the ring-down signals were plotted and are shown in Figure 2. The linearity of the ring-down signal indicates no additional interferences were contained within the signal. Additionally, Figure 2 shows that when $NO_3^•$ is present, the expected subsequent decrease in the ring-down time (110.4 μs) was observed; in this case at a concentration of 124 ppt. For this system, the detection limit was determined to be 1.7 ppt. Due to environmental issues, such as barometric pressure, and the aging of the N_2O_5,[44,55] the $N_2O_5/NO_3^•$ concentration ratio leaving the trap can vary over time. Therefore, the feedback system is designed to maintain the concentration within the experiment chamber at ±30 ppt of that specified by the user.

The system determines τ_{empty} by generating a 5% RH atmosphere and calculating a 1 min rolling average for 30 min. This ring-down value is then stored in a data file and used for all subsequent experiments until a new value is measured. In practice, the user determines a new τ_{empty} prior to each experiment.

B. Drift of τ_{empty} over time

Huang and Lehmann observed that changes in barometric pressure can affect the ring-down times of a CRDS cavity.[55] For this system, several experiments were ran using clean air (no $NO_3^•$) at 5% RH for a period of 48 h or longer. Figure 3 shows the results of one such experiment. In this plot, the mean value for τ_{empty} is 140.3 μs with a standard deviation of 1.6 μs. As can be seen in Table I, the standard deviations range from 1.0 to 2.9. In the worst case, with a standard deviation of 2.9 μs, the calculated error is ±11 ppt (or 11%) for a target concentration of 100 ppt. Due to the system's ±30 ppt control band around the target concentration, the potential drift error becomes irrelevant.

C. $NO_3^•$ loss and target $NO_3^•$ determination

The results of the $NO_3^•$ loss experiments can be seen in Figure 4. N_2 flow rates through the trap gave overall percent $NO_3^•$ losses through the system for 5 ml min^{-1}, 10 m l min^{-1}, and 15 ml min^{-1} as 57.0% (±9.9), 50.2% (±12.9), and 41.5% (±10.6), respectively. The flow rates through the dilution chambers, CRDS cavity, and experiment chamber were held constant. Subsequent plots of the data indicated a linear relationship that can be described using Eq. (2). The decrease in percentage loss of $NO_3^•$ at higher flow rates can be attributed to the limited uptake capacity of the Teflon tubing walls, as previously described by Dube *et al.*[29]

$$\%NO_3^{\bullet}\ \text{loss} = 1.55(N_2\ \text{flow rate}) + 65.04, \quad (2)$$

$$NO_3^{\bullet}\ (\text{ideal}) = NO_3^{\bullet}\ (\text{specified}) / (1.00 - \%NO_3^{\bullet}\ \text{loss}). \quad (3)$$

Using Eq. (2), the system determines the loss based upon the N_2 flow rate through the trap. Using Eq. (3), the system then determines the ideal measurement from the CRDS to produce the desired $NO_3^{\bullet}$ concentration (i.e., 100 ppt) within the experiment chamber. The difference between the actual measured concentration and the ideal measured concentration is the feedback provided to the PID control algorithm.

Figure 5 shows the data from one 72 h experiment. The green data points indicate the ideal concentration to be measured by the CRDS based upon Eq. (3), which changes as the flow of N_2 through the N_2O_5 trap changes. The red data points show the actual concentration measured by the CRDS. As can be seen, the concentration fluctuates but the system adjusts flows in order to maintain it. These flow adjustments result in the changes seen in the green data. The blue data indicate the calculated $NO_3^{\bullet}$ concentration within the experiment chamber, which is specified at 100 ppt, ±30 ppt. The fluctuations in the calculated $NO_3^{\bullet}$ concentration within the experiment chamber (blue) are significantly less than those shown by the measured concentration (red). This is due to the large amount of $NO_3^{\bullet}$ lost (40%–60%), as calculated from Eqs. (2) and (3).

D. Indoor nitrate radical surface chemistry

Indoor environment models by Sarwar *et al.*[56] and recent measurements by Nøjgaard[12] indicate that $NO_3^{\bullet}$ exists indoors in the 1–60 ppt range. At these concentrations and given a typical air exchange 0.6 h^{-1},[57] gas-phase reactions of $NO_3^{\bullet}$ with VOCs/SVOCs are important. For example, $NO_3^{\bullet}$ reactions with terpenes such as limonene, terpinolene, and α-terpinene have pseudo-first order rate constants of 1.1, 8.6, and 16 h^{-1}, respectively.[58] This data suggests that these reactions will likely occur before removal by air exchange leading to the formation of oxidation products indoors. However, surface-phase reactions may be more influential indoors than gas-phase reactions as air exchange becomes less important. Furthermore, research has shown that several surface-bound species have higher reaction probabilities than their respective gas-phase reactions.[59]

V. Conclusions

The novel SCRADES is able to generate $NO_3^{\bullet}$ at specified concentrations (50–500 ppt) and at specified flow rates (500– 2000 ml min^{-1}) to the experiment chamber for over 72 h. This system will be used to deliver $NO_3^{\bullet}$ at concentrations that exist indoors in order to initiate reactions on a variety of indoor surfaces. Initial experiments have focused on low humidity (i.e., 5%) in order to reduce loss of $NO_3^{\bullet}$ due to reactions with water. Future tests of the system will include increasing the RH to 50% in order to mimic typical indoor air conditions. Data from these experiments will be useful in developing more accurate exposure assessments, better analytical tools for health hazard evaluations and industrial hygiene sampling, and improved engineering control methods to reduce chemical contaminants.

Acknowledgments

The findings and conclusions in this report are those of the author(s) and do not necessarily represent the official position of the Centers for Disease Control and Prevention.

References

1. Weschler CJ. Indoor Air. 2011; 21:205. [PubMed: 21281360]
2. Atkinson R, Arey J. Chem Rev. 2003; 103:4605. [PubMed: 14664626]
3. Atkinson R, Plum CN, Carter WPL, Winer AM, Pitts JN. J Phys Chem. 1984; 88:1210.
4. Atkinson R, Tuazon EC, Aschmann SM. Environ Sci Technol. 1995; 29:1860. [PubMed: 22176461]
5. Forester CD, Ham JE, Wells JR. Atmos Environ. 2007; 41:1188.
6. Jones BT, Ham JE. Atmos Environ. 2008; 42:6689.
7. Wells JR. Environ Sci Technol. 2005; 39:6937. [PubMed: 16201614]
8. Weschler CJ. Sci World J. 2001; 1:443.
9. Weschler CJ. Indoor Air. 2004; 14:184. [PubMed: 15330786]
10. Finlayson-Pitts, BJ.; Pitts, JJN. Chemistry of the Upper and Lower Atmosphere. Academic; New York: 2000. p. 8
11. Seinfeld, JH.; Spandis, SN. Atmospheric Chemistry and Physics. Wiley; NJ: 2006. p. 250
12. Nojgaard JK. Chemosphere. 2010; 79:898. [PubMed: 20304460]
13. Brown SS, Dube WP, Osthoff HD, Stutz J, Ryerson TB, Wollny AG, Brock CA, Warneke C, De Gouw JA, Atlas E, Neuman JA, Holloway JS, Lerner BM, Williams EJ, Kuster WC, Goldan PD, Angevine WM, Trainer M, Fehsenfeld FC, Ravishankara AR. J Geophys Res, [Atmos]. 2007; 112:17.10.1029/2007JD008883
14. Ishiwata T, Fujiwara I, Naruge Y, Obi K, Tanaka I. J Phys Chem. 1983; 87:1349.
15. Ishiwata T, Tanaka I, Kawaguchi K, Hirota E. Bull Soc Chim Belg. 1983; 92:502.
16. Matsumoto J, Kosugi N, Imai H, Kajii Y. Rev Sci Instrum. 2005; 76:064101.
17. Wood EC, Wooldridge PJ, Freese JH, Albrecht T, Cohen RC. Environ Sci Technol. 2003; 37:5732. [PubMed: 14717187]
18. Allan BJ, Plane JMC, Coe H, Shillito J. J Geophys Res, [Atmos]. 2002; 107:4588.10.1029/2002jd002112
19. Biermann HW, Winer AM, Pitts JN. Abstr Pap - Am Chem Soc. 1986; 192:144.
20. Geyer A, Alicke B, Ackermann R, Martinez M, Harder H, Brune W, di Carlo P, Williams E, Jobson T, Hall S, Shetter R, Stutz J. J Geophys Res, [Atmos]. 2003; 108:4368.10.1029/2002jd002967
21. Li S, Liu W, Xie P, Li A, Qin M, Dou K. Adv Atmos Sci. 2007; 24:875.
22. Stutz J, Alicke B, Ackermann R, Geyer A, White A, Williams E. J Geophys Res, [Atmos]. 2004; 109:D12306.10.1029/2003jd004209
23. Stutz J, Wong KW, Lawrence L, Ziemba L, Flynn JH, Rappenglueck B, Lefer B. Atmos Environ. 2010; 44:4099.
24. von Friedeburg C, Wagner T, Geyer A, Kaiser N, Vogel B, Vogel H, Platt U. J Geophys Res, [Atmos]. 2002; 107:4168.10.1029/2001jd000481
25. Mentel TF, Bleilebens D, Wahner A. Atmos Chem Phys. 1996; 30:4007.
26. Ayers JD, Apodaca RL, Simpson WR, Baer DS. Appl Opt. 2005; 44:7239. [PubMed: 16318196]
27. Brown SS, Stark H, Ciciora SJ, McLaughlin RJ, Ravishankara AR. Rev Sci Instrum. 2002; 73:3291.
28. Brown SS, Stark H, Ravishankara AR. Appl Phys B. 2002; 75:173.
29. Dube WP, Brown SS, Osthoff HD, Nunley MR, Ciciora SJ, Paris MW, McLaughlin RJ, Ravishankara AR. Rev Sci Instrum. 2006; 77:034101.
30. Odame-Ankrah CA, Osthoff HD. Appl Spectrosc. 2011; 65:1260. [PubMed: 22054085]

31. Wagner NL, Dube WP, Washenfelder RA, Young CJ, Pollack IB, Ryerson TB, Brown SS. Atmos Meas Tech. 2011; 4:1227.
32. Disselkamp RS, Carpenter MA, Cowin JP, Berkowitz CM, Chapman EG, Zaveri RA, Laulainen NS. J Geophys Res, [Atmos]. 2000; 105:9767.10.1029/1999JD901189
33. Gratpanche F, Sawerysyn JP. J Chim Phys Phys Chim Biol. 1999; 96:213.
34. Grossi CM, Brimblecombe P. J Phys Iv. 2002; 12:197.
35. Ham JE, Wells JR. Indoor Air. 2008; 18:394. [PubMed: 18647191]
36. Ham JE, Wells JR. Atmos Environ. 2009; 43:4023.
37. Ham JE, Wells JR. Chemosphere. 2011; 83:327. [PubMed: 21237482]
38. Reiss R, Ryan PB, Koutrakis P, Tibbetts SJ. Environ Sci Technol. 1995; 29:1906. [PubMed: 22191336]
39. Shu S, Morrison GC. Environ Sci Technol. 2011; 45:4285. [PubMed: 21517064]
40. Shu S, Morrison GC. Atmos Environ. 2012; 47:421.
41. Springs M, Wells JR, Morrison GC. Indoor Air. 2011; 21:319. [PubMed: 21204992]
42. Toftum J, Feund S, Salthammer T, Weschler CJ. Atmos Environ. 2008; 42:7632.
43. Flemmer MM, Ham JE, Wells JR. Rev Sci Instrum. 2007; 78:014101. [PubMed: 17503934]
44. Perraud V, Bruns EA, Ezell MJ, Johnson SN, Greaves J, Finlayson-Pitts BJ. Environ Sci Technol. 2010; 44:5887. [PubMed: 20608721]
45. McDaniel AH, Davidson JA, Cantrell CA, Shetter RE, Calvert JG. J Phys Chem. 1988; 92:4172.
46. Brown SS. Chem Rev. 2003; 103:5219. [PubMed: 14664649]
47. Clemitshaw KC. Crit Rev Environ Sci Technol. 2004; 34:1.
48. Fiddler MN, Begashaw I, Mickens MA, Collingwood MS, Assefa Z, Bililign S. Sensors. 2009; 9:10447. [PubMed: 22303184]
49. Friedrichs G, Phys Z. Chem-Int J Res Phys Chem Chem Phys. 2008; 222:31.
50. Paldus BA, Kachanov AA. Can J Phys. 2005; 83:975.
51. Scherer JJ, Paul JB, Collier CP, Okeefe A, Rakestraw DJ, Saykally RJ. Spectroscopy. 1996; 11:46.
52. Scherer JJ, Paul JB, Okeefe A, Saykally RJ. Chem Rev. 1997; 97:25. [PubMed: 11848864]
53. Keller-Rudek, H.; Moortgat, GK. Mainz; Germany: 2012. MPI-Mainz-UV-Vis Spectral Atlas of Gaseous Molecules. see http://www.atmosphere.mpg.de/enid/2295
54. Fuchs H, Dube WP, Cicioira SJ, Brown SS. Anal Chem. 2008; 80:6010. [PubMed: 18588318]
55. Huang HF, Lehmann KK. Appl Opt. 2010; 49:1378. [PubMed: 20220895]
56. Sarwar, G.; Corsi, R.; Allen, D.; Weschler, CJ. Indoor Air 2002. Vol. 2002. Monterey, CA: 2002. p. 80
57. Wilson AL, Colome SD, Tian Y, Becker EW, Baker PE, Behrens DW, Billick IH, Garrison CA. J Expo Anal Environ Epidemiol. 1996; 6:311. [PubMed: 8889951]
58. Nazaroff WW, Weschler CJ. Atmos Environ. 2004; 38:2841.
59. Voges AB, Stokes GY, Gibbs-Davis JM, Lettan RB, Bertin PA, Pike RC, Nguyen ST, Scheidt KA, Geiger FM. J Phys Chem C. 2007; 111:1567.

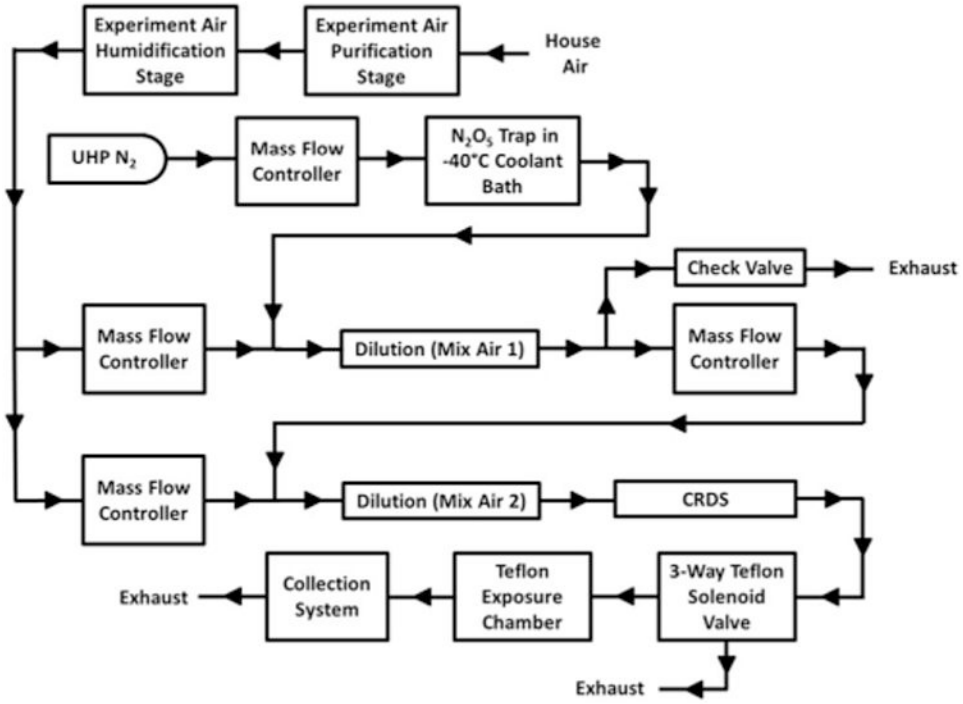

Fig. 1.

Flow diagram of the surface chemistry reactant air delivery and experiment system (SCRADES).

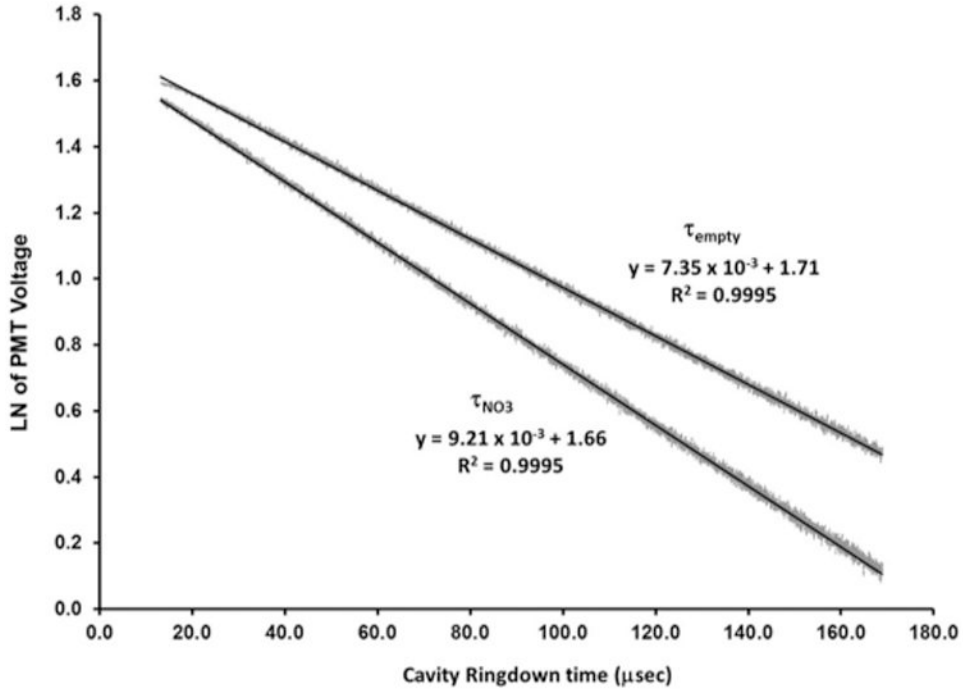

Fig. 2.

Log plots of ring-down traces for τ_{empty} (no $NO_3^{\bullet}$) and τ_{NO_3} (124 ppt $NO_3^{\bullet}$) with linear fit.

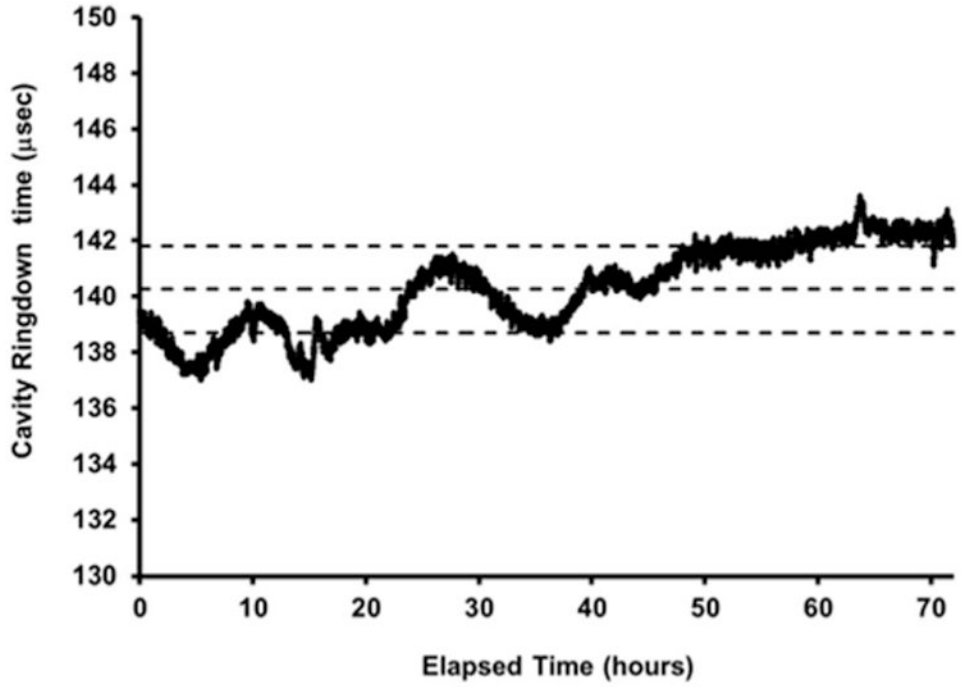

Fig. 3.

Drift of τ_{empty} over a 72 h period with mean ring-down time (140.3 μs) bracketed by standard deviation (±1.6).

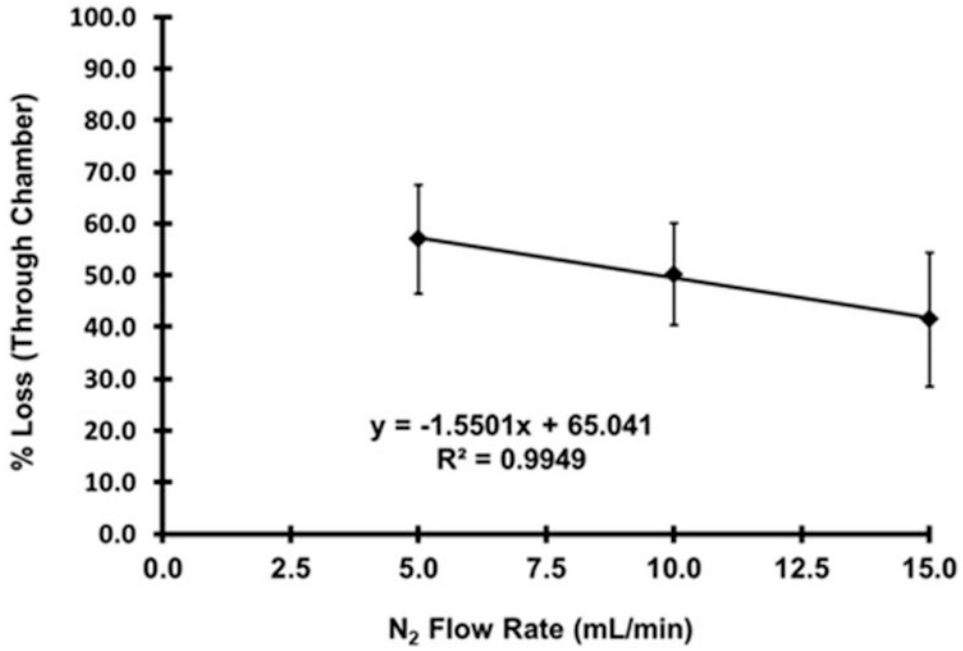

Fig. 4.

Percent loss of $NO_3^{\bullet}$ between the CRDS cavity and the experiment chamber based on N_2 flow through the N_2O_5 trap. Error bars represent the standard deviations from five separate experiments at each flow rate.

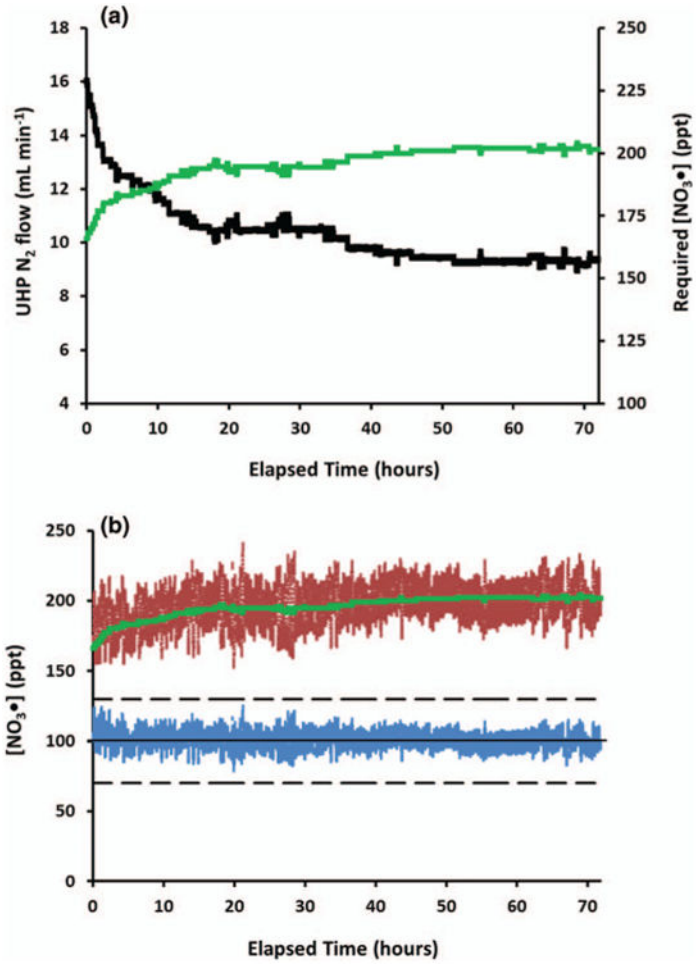

Fig. 5.

Calculated ideal $NO_3^{\bullet}$ concentration to be measured by CRDS based on N_2 flow through N_2O_5 trap (green). Actual $NO_3^{\bullet}$ concentration measured by CRDS (red). Calculated $NO_3^{\bullet}$ concentration in experiment chamber (blue).

Table I

Results of CRDS τ_{empty} (no $NO_3^{\bullet}$) drift experiments.

	Experiment 1	Experiment 2	Experiment 3	Experiment 4	Experiment 5
Elapsed time (hours)	48	67	96	72	72
τ_{empty}	147.5	137.5	141.2	149.6	140.3
Average (s.d.) (μs)	(±2.9)	(±2.5)	(±2.9)	(±1.0)	(±1.6)